Applying molecular simulation to the analysis of lipid monolayer reflectometry

A. R. McCluskey,[1, 2, *] J. Grant,[3] A. J. Smith,[2] J. L. Rawle,[2] D.
J. Barlow,[4] M. J. Lawrence,[5] S. C. Parker,[1] and K. J. Edler[1, †]

[1]*Department of Chemistry, University of Bath, Claverton Down, Bath, BA2 7AY, UK*
[2]*Diamond Light Source, Harwell Campus, Didcot, OX11 0DE, UK*
[3]*Computing Services, University of Bath, Claverton Down, Bath, BA2 7AY, UK*
[4]*Institute of Pharmaceutical Science, King's College London, London, SE1 9NH, UK*
[5]*Division of Pharmacy and Optometry, University of Manchester, Manchester, M13 9PT, UK*
(Dated: January 10, 2019)

Using molecular simulation to aid in the analysis of neutron reflectometry measurements is commonplace. However, reflectometry is a tool to probe large-scale structures, and therefore the use of all-atom simulation may be unjustified. This work presents the first direct comparision between the reflectometry profiles obtained from different all-atom and coarse-grained molecular dynamics simulations. These are compared with a traditional layer model analysis method to determine the minimum simulation resolution required to accurately reproduce experimental data. We find that systematic problems limit the efficacy of the MARTINI potential model, while the Berger united-atom and Slipids all-atom potential models agree similarly well with the experimental data. The traditional layer model gives the best agreement, however the higher resolution simulation-dependent methods produce agreement that is only slightly worse.

I. INTRODUCTION

Neutron and X-ray reflectometry techniques are popular in the study of nanolayered structures, such as polyelectrolyte-surfactant mixtures [1], lipid bilayer systems [2], electrodeposited films [3], and dye-sensitised solar cell materials [4]. Unlike other surface-sensitive techniques, such as atomic force microscopy (AFM) or scanning electron microscopy (SEM), reflectometry methods can investigate buried interfaces in addition to the material surface. This is due to the ability of neutrons and X-rays to probe more deeply into a material than an AFM tip or the electron. Additionally, reflectometry techniques can more easily provide information about the average structure of a material over large regions of space, resulting in significantly improved sampling, compared with microscopy techniques [5].

The growth in popularity of reflectometry techniques can be attributed to the significant development of reflectometry instrumentation, such as FIGARO, the horizontal neutron reflectometer at the ILL [6], and the beam deflection system at the I07 beamline of the Diamond Light Source [7]. These have enabled the study of more complex systems including biomimetic bacterial membrane [8], and polymeric energy materials [9]. However, the ability to study complex systems poses an important data analysis challenge, where a typical layer model approach may not be sufficient.

The Abelès matrix formalism for stratified media [10], is the most commonly applied method to analyse reflectometry data from a surfactant monolayer. This model-dependent approach involves the construction of a layer model to describe the system under study. The reflectometry profile is then calculated from the model, and the model refined to improve agreement between the calculated reflectometry profile and that measured experimentally. Such an approach is discussed in detail in the work of Campbell *et al.* [11], where they investigate the different approaches to the analysis of surfactant monolayers.

The Abelès matrix formalism is often described as the dynamical approach to reflectometry analysis, in contrast to the Fourier transform-based kinematic approach [12, 13]. The dynamical approach considers the reflection and refraction of the probing radiation at a series of interfaces, where the refractive index is a function of the scattering length densities (SLDs) for each layer. By considering Figure 1 it is clear how the reflected radiation could interact coherently and incoherently by analogy with Bragg's law.
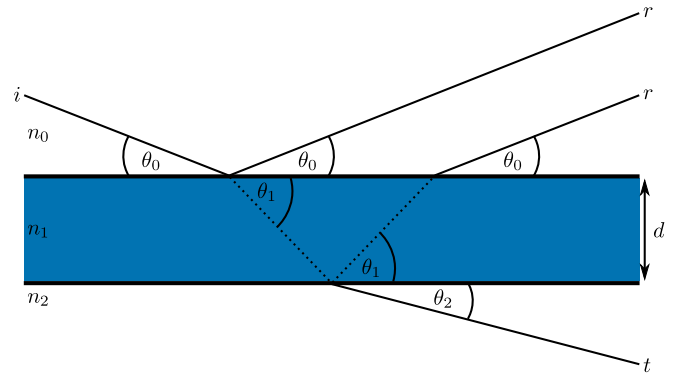

FIG. 1. A schematic of a reflectometry experiment, where i is the incident radiation, r is the reflected radiation, t is the transmitted radiation, and d is the layer thickness, for each layer n, and the angles of incidence, reflection, and transmittence all depend on Snell's law.

* a.r.mccluskey@bath.ac.uk

† k.edler@bath.ac.uk

A commonly suggested method for the multi-modal analysis of reflectometry measurements is the use of molecular dynamics (MD) simulations. MD-driven multi-modal analysis has been applied previously, either by the calculation of the SLD profile from the simulation or the full determination of the reflectometry profile. In the former case, the calculated SLD profile may be compared with the SLD profile determined from the use of a traditional analysis method. Bobone *et al.* used such a method to study the antimicrobial peptide trichogin GA-IV within a supported lipid bilayer [14]. A four layer model consisting of the hydrated SiO_2 layer, an inner lipid head-region, a lipid tail-region, and an outer lipid head region was used in the Abelès matrix formalism. The SLD profile from the MD simulations agreed well with that fitted to the reflectometry data from the layer model.

The reflectometry profile was calculated explicitly from classical simulation in the works of Miller *et al.* and Anderson and Wilson [15, 16]. In these, an amphiphilic polymer at the oil-water interface was simulated by Monte Carlo and MD respectively, and the neutron reflectometry profile for found by splitting the simulation cell into a series of small layers and applying the Abelès matrix formalism. There was good agreement between the experimental and calculated reflectometry, for low interface coverages of the polymer. Another work that has made direct comparison between the atomistic simulation-derived reflectometry and those measured experimentally includes that of Darré *et al.* [17]. In this work, NeutronRefTools was developed to produce the neutron reflectometry profile from a given MD simulation. The particular system studied was a supported 1,2-dimyristoyl-*sn*-glycero-3-phosphocholine (DMPC) lipid bilayer, with good agreement found between the simulation-derived profile and the experimental measurement. However, the nature of the support required a correction for the head-group hydration to be imposed to achieve this agreement.

Koutsioubas used the MARTINI coarse-grained representation of a 1,2-dipalmitoyl-*sn*-glycero-3-phosphocholine (DPPC) lipid bilayer to compare with experimental reflectometry [18]. This work shows that the parameterisation of the MARTINI water bead was extremely important in the reproduction of the reflectometry data, as the non-polarisable water bead would freeze into crystalline sheets resulting in artefacts in the reflectometry profiles calculated. The work of Hughes *et al.* studied again a DPPC lipid bilayer system [19], albeit an all-atom representation, that was compared with a supported DPPC lipid bilayer system measured with polarised neutron reflectometry. The SLD profile found from MD was varied to better fit the experimental measurement, resulting in good agreement. Additionally, the variation of the SLD profile was used to remove artefacts that arose from poor splicing between the MD simulations that the layer model used in regions such as the gold and magnetic permalloy layers not present in the simulation.

In all of the examples discussed so far there is no direct comparison between the reflectometry profile determined from simulation and that from the application of a traditional analysis method. Indeed, the only example, to the authors' knowledge where direct comparison was drawn is the work of Dabkowska *et al.* [20]. This work compares the reflectometry profile from a DPPC monolayer at the air-water interface containing dimethyl sulfoxide molecules with a similar molecular dynamics simulation parameterised with the CHARMM potential model. The use of multimodal analysis allowed the determination of the position of a concentration of DMSO molecules at a particle region within a monolayer and the orientation of such molecules.

Herein, we present the comparison of three MD simulations of different potential models, with different particle grain-sizes; namely the Slipid all-atom [21], Berger united-atom [22], and MARTINI coarse-grained potential models [23]. We believe that this work offers a fundemental insight into the simulation resolution that is required to reproduce experimental neutron reflectometry measurements. Furthermore, we suggest some adjustments that may be made to the more traditional, layer models that are commonly used to analyse such measurements.

II. METHODOLOGY

A. Neutron reflectometry measurements

The neutron reflectometry measurements analysed in this work have been previously published by Hollinshead *et al.* [24], and full details of the methods used can be found in the previous publication. These measurements involved studying seven contrasts of 1,2-distearoyl-*sn*-phosphatidylcholine (DSPC) at the air-water interface (Table I), at four different surface pressures; $20\,\mathrm{mN\,m^{-1}}$ to $50\,\mathrm{mN\,m^{-1}}$.

TABLE I. The different contrasts of lipid and water investigated in this work. ACMW is air-contrast matched water, where D_2O and H_2O are mixed so as to given a water with a SLD of zero.

Shorthand	Lipid contrast	Water contrast
h-D_2O	h-DSPC	D_2O
d_{13}-ACMW	d_{13}-DSPC	ACMW
d_{13}-D_2O	d_{13}-DSPC	D_2O
d_{70}-ACMW	d_{70}-DSPC	ACMW
d_{70}-D_2O	d_{70}-DSPC	D_2O
d_{83}-ACMW	d_{83}-DSPC	ACMW
d_{83}-D_2O	d_{83}-DSPC	D_2O

B. Molecular dynamics simulations

The DSPC monolayer simulations were made up of lipid molecules modelled with three potential models, each of a different particle grain-size. The Slipids potential model is an all-atom representation of the lipid molecules [21], which was used alongside the single point charge (SPC) water model [25], with a timestep of 0.5 fs. The Berger potential model is obtained by the integration of the hydrogen atoms to produce a united atom potential model [22]; again the SPC water molecules were used. The removal of the high frequency C−H bonds allows for the timestep to be increased to 1 fs. Finally, the lowest resolution potential model used was the MARTINI [23] alongside the polarisable MARTINI water model [26], to avoid the freezing issues observed previously [18]. The MARTINI 4-to-1 heavy atom beading allows for the use of a 20 fs timestep. All simulations were conducted with temperature coupling to a heat bath at 300 K and a leap-frog integrator, and run using GROMACS 5.0.5 [27–30] on 32 cores of the STFC Scientific Computing resource SCARF. The simulation was of a monolayer, therefore the Ewald 3DC correction was applied to allow for the use of x/y-only periodic boundary conditions [31]. A close-packed "wall" of non-interacting dummy atoms was placed at each side of the simulation cell in the z-direction to ensure that the atoms could not leave the simulation cell.

The starting simulation structure was generated using the molecular packing software Packmol [32]. This was used to produce a monolayer of 100 DSPC molecules, with the head group oriented to the bottom of the simulation cell. A 6 Å layer of water was then added such that the head groups were overlapping, this was achieved using the `solvate` functionality in GROMACS 5.0.5. Examples of the dry and wet monolayer can be seen in Figure 2 for the Berger potential model system. A general protocol was then used to relax the system at the desired surface coverage, reproducing the effects of a Langmuir trough *in silico*. This involved subjecting the system to a semi-isotropic barostats, with a compressibility of $4.5 \times 10^{-5}\,\mathrm{bar}^{-1}$ of the Slipids and Berger simulations and $3.0 \times 10^{-4}\,\mathrm{bar}^{-1}$ for the MARTINI simulations. The pressure in the z-dimension was kept constant at 1 bar, while it was increased in the x- and y-dimensions isotropically. When the xy-surface area is reached that is associated with the area per molecule (APM) for each surface pressure, described by the experimental surface pressure-isotherm (Figure 3), given in Table II, the coordinates were saved and used as the starting structure for the equilibration simulation. This involved continuing the use of the semi-isotropic barostat, with the xy-area of the box fixed, allowing the system to relax at a pressure of 1 bar in the z-dimension. The equilibration period was 1 ns, following which the 50 ns NVT ensemble production simulations were run, on which all analyses were conducted.
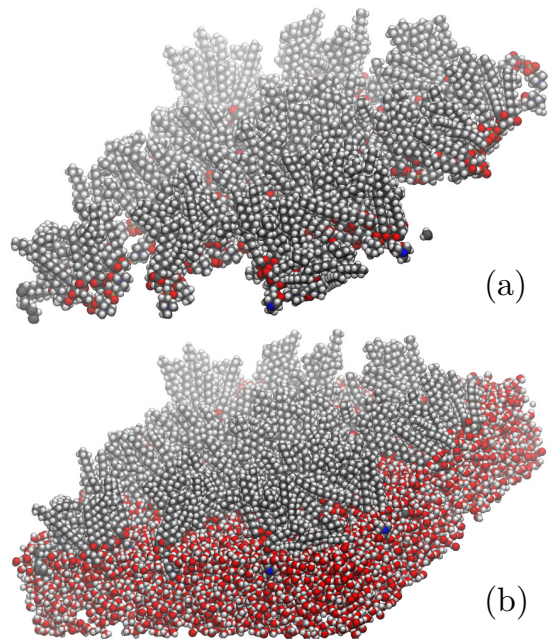

FIG. 2. The DSPC monolayer (a) without water layer and (b) with water layer, visualised using VMD[33].
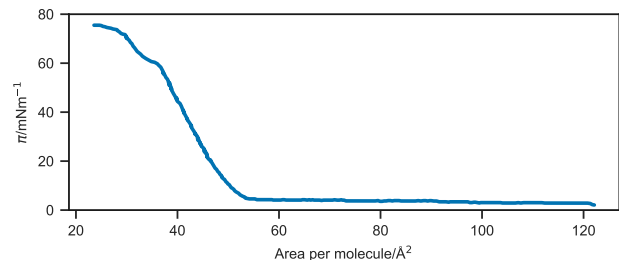

FIG. 3. The experimental surface pressure isotherm for DSPC, taken from the work of Kubo *et al.*[34].

C. Abelès matrix formalism

To compare against the simulation-derived reflectometry profiles, the chemically-consistent surfactant monolayer model was used [35, 36]. This model is implemented as a class that is compatible with the Python package refnx [37, 38]. The model is made up of two layers; the head-layer at the interface with the solvent and the tail-layer at the interface with the air. The head components have a calculated scattering length, b_h, (found as a summation of the neutron scattering lengths of the individual atoms, see Table S1) and a component volume, V_h. These make up a head-layer with a given thickness, d_h, and interfacial roughness, σ_h, and within this layer some volume fraction of solvent may intercalate, ϕ_h. The tail components also have a similarly calculated scattering length, b_t, and component volume, V_t. In this work, the fully extended length of the hydrocarbon tail, t_t, as

TABLE II. The areas per molecule (APM) associated with particular surface pressures and the size of the x- and y-cell dimension for a simulation of 100 lipid molecules.

$\pi/\mathrm{mN\,m^{-1}}$	APM/Å^2	xy-cell length/Å
20	47.9	69.1
30	46.4	68.1
40	45.0	67.1
50	44.6	66.0

defined by the Tanford Equation [39],

$$t_t = 1.54 + 1.265n, \tag{1}$$

where n is the number of carbon atoms in the chain, and so for DSPC $t_t = 24.3\,\text{Å}$. The tail-layer thickness is then found by considering t_t and the angle that the chain is tilted by with respect to the interface normal, θ_t,

$$d_t = t_t \cos\theta_t. \tag{2}$$

This was used to impose a chemically-consistent maximum on the thickenss of the tail-layer, e.g. it cannot be thicker than the maximum extended tail length of the lipid. The SLD of the tail and head layers used in the Abelès matrix formalism can therefore be found as,

$$\mathrm{SLD}_i = \frac{b_i}{V_i}(1 - \phi_i) + \mathrm{SLD}_s(\phi_i), \tag{3}$$

where, SLD_s is the scattering length density of the subphase (water), and i indicates either the tail- or head-layer; it is assumed that the tail layer contains no solvent or air, e.g. $\phi_t = 0$ in agreement with the work of Campbell $et\ al.$ [11]. To ensure that the number density of the head components and pairs of tail components is the same, the following constraint was included in the model [40],

$$\phi_h = 1 - \left(\frac{d_t V_h}{V_t d_h}\right). \tag{4}$$

A single value for the interfacial roughness was fit for all interfaces, as there is only a single lipid type in each monolayer [11]. Therefore, any conformal roughness at the air-water interface is carried equally through all the layers. The only modification made to this monolayer model used previously was that the tail component volume was also constrained, based on the APM (taken from the surface pressure isotherm),

$$V_t = d_t\mathrm{APM}. \tag{5}$$

The result of this is that both the monolayer model and the simulation-derived models were constrained equally by this calculated surface coverage.

In this work, the experimental data from all seven contrasts were co-refined to a single monolayer model, where the head thickness, chain tilt angle, head component volume, and interfacial roughness were allowed to vary. The values of the head and tail scattering lengths, along with the super and subphase SLDs are given in Table S1. The length of the tail chain was kept constant at 24.3 Å, as defined by the Tanford equation [39]. This is due to the monolayer being investigated at relatively high surface pressures, where the extended, all-trans conformations are likely to be present. For each co-refinement of seven neutron reflectometry measurements, there were in total five degrees of freedom in the fitting process. The Abelès matrix formalism was used to calculate the reflectometry profiles as described in the ESI.

D. Simulation-derived analysis

Version 1.0.1 of refnx [37, 38] includes the ability to obtain simulation-derived reflectometry profiles, using a similar method to that employed in previous work, such as Dabkowska $et\ al.$ [20]. The Abelès matrix formalism is applied to layers (see ESI), the SLD of which is drawn directly from the simulation, and the thickness of which is defined. The layer thickness used was 1 Å for the Slipid and Berger potential model simulations, with an interfacial roughness between these layers is defined as 0 Å. For the MARTINI potential model, a layer thickness of 4 Å was used, with an interfacial roughness of 0.8 Å, a detailed discussion for the rationale behind this is available in the ESI. Each of the 50 ns production simulations were analysed with a frequency of every 0.1 ns, and the SLD profiles were determined by summing the scattering lengths, b_j, for each of the atoms in a given layer.

$$\mathrm{SLD}_n = \frac{\sum_j b_j}{V_n}, \tag{6}$$

where, V_n is the volume of the layer n, obtained from the simulation cell parameters in the plane of the interface and the defined layer thickness. A uniform background and scale factor were then determined using refnx to offer the best agreement between the calculated reflectometry profile and that measured experimentally.

E. Comparison between monolayer model and simulation-derived analysis

In order to assess the agreement between the models from each method, the following goodness-of-fit metric was used, following the transformation of the data into Rq^4 space,

$$\chi^2 = \sum_{i=1}^{N_{\mathrm{data}}} \frac{[R_{\exp}(q_i) - R_{\sim}(q_i)]^2}{[\delta R_{\exp}(q_i)]^2}, \tag{7}$$

where q_i is a given q-vector, which depends on the neutron wavelength and reflected angle, $R_{\exp}(q_i)$ is the experimental reflected intensity, $R_{\sim}(q_i)$ is the simulation-derived reflected intensity, and $\delta R_{\exp}(q_i)$ is the resolution function of the data.

Parameteric outcomes from the different analysis methods were also compared, such as the number of water molecules per head group, wph. This was obtained from the monolayer model by considering the solvent fraction in the head-layer, ϕ_h, the volume of the head group, V_h, and taking the volume of a single water molecule to be $29.9\,\text{Å}^3$ (from the density of water as $997\,\text{kg}\,\text{m}^{-3}$),

$$\text{wph} = \frac{\phi_h V_h}{29.9 - 29.9\phi_h}. \tag{8}$$

From the molecular dynamics simulation, the number densities for each component of the system were determined. The ratio of the integrals of the lipid heads and the water then gave the wph. The range for this integral was taken as between the 20 % and 80 % quantiles of the lipid head-layers.

It was also possible to compare the tilt of the lipid tails with respect to the surface normal. This angle was used as a fitting parameter in the monolayer model, and can be obtained directly from the MD simulation. For this, a vector was defined between the first and last carbon atoms of each chain and the angle with respect to the surface normal was found trigonometrically.

III. RESULTS & DISCUSSION

Figure 4 compares the reflectometry and SLD profiles from each of the different methods used at a surface pressure of $30\,\text{mN}\,\text{m}^{-1}$. The data for the other surface pressures showed similar trends, and can be found in the ESI. The χ^2 goodness-of-fit metric between the calculated and experimental reflectometry is given in Table III for each contrast, in addition to the average χ^2 and a standard deviation.

A. Comparison of MARTINI

It is clear from Figure 4 and Table III, that the MARTINI potential model simulations very poorly reproduce the reflectometry profile. Furthermore, it is noted that the agreement with the contrasts containing D_2O are particularly poor. This is most likely an artefact of the structuring effect from the wall at the bottom of the simulation cell on the polarisable MARTINI water. It is noted that this may be reduced through the use of a less-ordered wall structure [18]. Another outstanding artefact present in the MARTINI potential model simulations is that the calculated length of the hydrocarbon tail from the simulation was found to be $16.87^{+1.77}_{-2.16}\,\text{Å}$, which is significantly less than the $24.3\,\text{Å}$ estimated by the Tanford equation. This is due to the nature of the MARTINI's 4-to-1 beading process, as DSPC has a hydrocarbon tail consisting of 18 carbon atoms, not possible to bead such a chain accurately with the MARTINI potential model..

In this work, a MARTINI lipid molecule was used with 4 MARTINI beads making up the chain; corresponding to an all-atom hydrocarbon chain of 16 atoms. Applying the Tanford equation to a hydrocarbon chain of such a length results in an anticipated length of $18.7\,\text{Å}$, which agrees better with that found from simulation.

The requirement for a 4-to-1 beading structre of the MARTINI potential model is a significant weakness in this work. A better method may involve the use of a 2-to-1 beading model. However, we are not aware of an off-the-shelf 2-to-1 coarse-grained potential model that is commonly applied to lipid molecules.

B. Comparison of other simulations

Table III shows that both the Slipid and Berger potential models agree well with the experimental data, with the Slipid potential model offering a slight improvement over the Berger. The quality of agreement between these higher-resolution potential models and the monolayer model is relatively similar. However, the monolayer model is still better than those determined from MD simulation. This is to be expected though, simply by considering the level of constraint present implicitly when determining the reflecometry profile directly from simulation. While the monolayer model constrains the layer model to be chemically-consistent, those from MD simulation have real chemical constraints present in the simulation; e.g. the bonding of atoms, and the non-bonded potentials. The quality of the agreement from this multimodal analysis technique it sufficient for such a method to be applied regularly in the analysis of neutron reflectometry.

Both the Slipid and Berger simulations produced values for the tail length that were in better agreement with the Tanford equation than the MARTINI simulation. For the Slipid simulation the tail length was found to be $19.91^{+1.65}_{-7.96}\,\text{Å}$, while for the Berger simulations a value of $19.41^{+1.96}_{-9.06}\,\text{Å}$ was obtained. Neither is quite as large as the $24.3\,\text{Å}$ from the Tanford equation, however it should be noted that this value is considered a maximum for the *fully extended* carbon tail. This is a possible indication that the assumption, made in the traditional analyis method, that the tail is fully extended may not be completely accurate.

Using the molecular dynamics simulations, and the monolayer model it is possible to compare the number of water molecules per head group. From the Slipids and Berger simulations, the number of water molecules per head group was found to be $7.85^{+0.59}_{-0.59}$ and $5.65^{+0.73}_{-0.52}$ respectively. These are in good agreement with the $5.47^{+0.84}_{-0.80}$ found from the monolayer model method in conjungtion with Equation 8.

It should be noted that to obtain the $50\,\text{ns}$ production run for the Slipids potential model simulation required over 13 days of using 32 cores of the SCARF computing resource. This is non-trivial and therefore not nec-
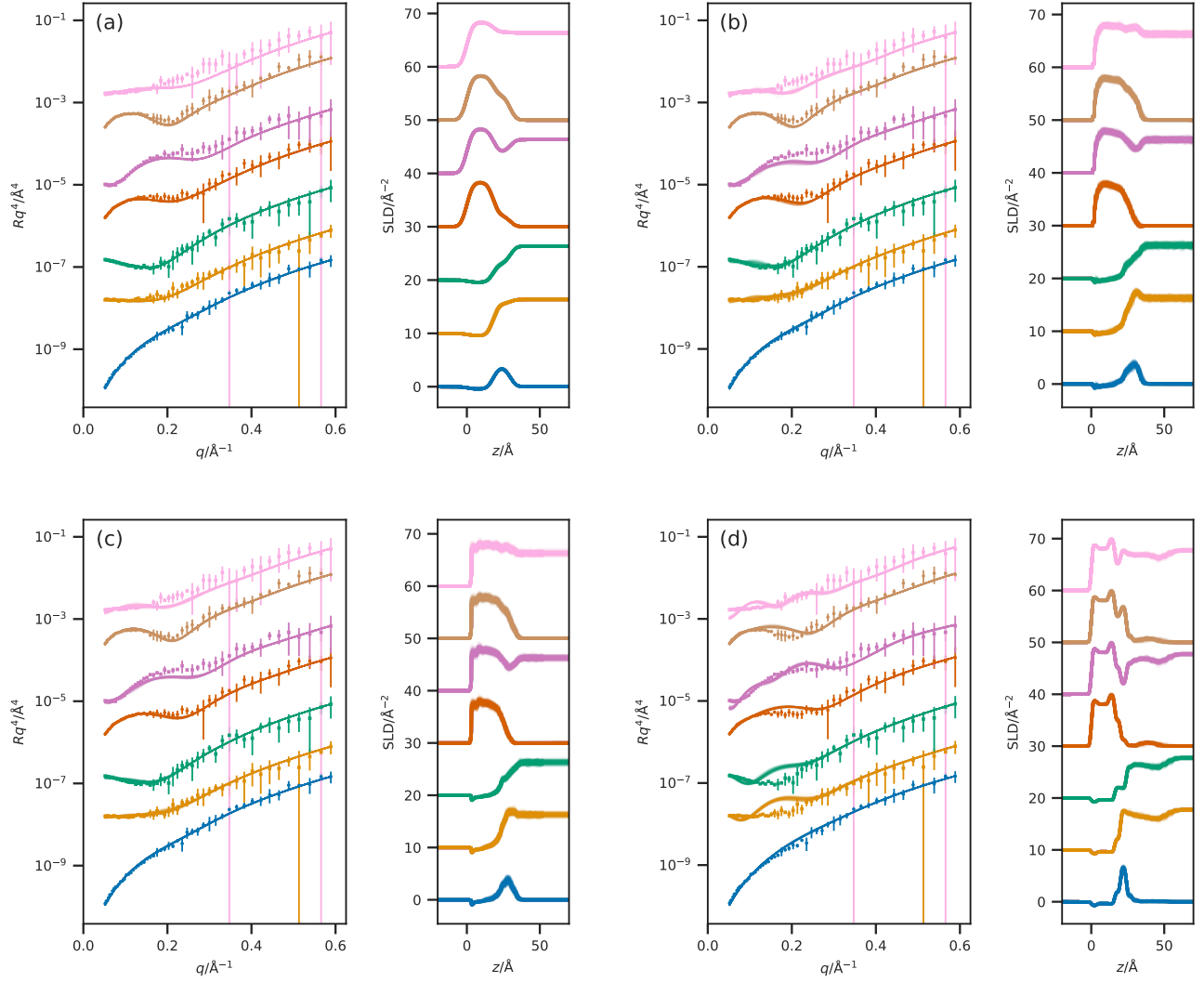
FIG. 4. A comparison of the reflectometry and SLD profiles obtained from (a) the monolayer model, (b) the Slipid simulation, (c) the Berger force-force simulation, and (d) the MARTINI potential model simulation at a surface pressure of $30\,\mathrm{mN\,m^{-1}}$. From top-to-bottom the contrasts are as follows; d_{83}-D_2O, d_{83}-ACMW, d_{70}-D_2O, d_{70}-ACMW, h-D_2O, d_{13}-D_2O, d_{13}-ACMW. The different contrast reflectometry profiles have been offset in the y-axis by an order of magnitude and the SLD profiles offset in the y-axis by $1 \times 10^{-6}\,\mathrm{\AA^{-2}}$, for clarity.

TABLE III. The goodness-of-fit between the calculated and experimental reflectometry profile at a surface pressure of $30\,\mathrm{mN\,m^{-1}}$.

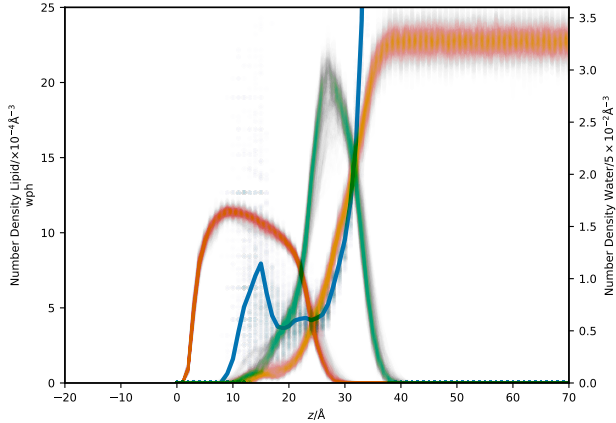| Contrast	Monolayer model	Slipid	Berger	MARTINI
h-D_2O	38.2	154.6	170.3	1565.3
d_{13}-ACMW	80.5	96.2	84.6	199.7
d_{13}-D_2O	84.1	214.5	122.6	2459.6
d_{70}-ACMW	141.8	76.0	88.7	436.5
d_{70}-D_2O	142.0	543.0	475.1	2198.2
d_{83}-ACMW	95.9	138.4	296.9	858.8
d_{83}-D_2O	344.1	400.2	486.5	3539.3
Average±Uncertainty	132.4 ± 92.8	231.8 ± 161.6	246.4 ± 162.4	1608.2 ± 1116.3

FIG. 5. The number density of each component; tails (orange), heads (green), water (yellow), and the number of water molecules per head group (blue dots, with the time-average shown as a solid blue line).

essarily applicable to all neutron reflectometry measurements. However, for the nearly as accurate Berger potential model simulations (which are only marginally less accurate), only approximately 2 days, of the same compute resource, were required. This suggests that given the quality of agreement with the experimental data achieved from the Berger potential model simulations it may be feasible to suggest simulations of such resolution may be run alongside experimental measurements at large facilities such as ISIS Neutron and Muon Source.

C. Using the Slipid simulations to improve the monolayer model

Despite the monolayer model offering a small improvement in agreement over the Slipid potential model simulation, we believe that it is possible to use these MD simulations to improve the existing monolayer model. An example of this has already been mentioned in terms of not applying the assumption that the carbon tail is fully extended. Another possible improvement can be found by considering Figure 5, which shows the water molecules per head group as a function of depth; it is clear that solvent penetration into the lipid head group area is not uniform. In particular, there is a clear pocket of water formed around the ester group of the lipid. This suggests that perhaps a different model for solvent penetration could be applied to the head layer to better describe the realistic solvent penetration.

It is generally suggested that the conformal roughness between layers should be carried evenly through the monolayer when there is only a single lipid type [11]. However, from Figure 5 it is clear that the overlap between the head-layer and water is much larger than that

between the tail and head. Furthermore, there is additionally some solvent present deep within the tail layer, due to the presence of head-group character in that region. While the interfacial roughness can be considered as describing the capillary wave form of the water surface, it is also frequently applied to account for the intrinsic/structural roughness in the monolayer that exists because of the fact that the lipid ensemble comprises molecules with different conformations and thus different chain lengths. This suggests that perhaps the constraint that the interfacial roughnesses should be constant through the monolayer might be relaxed.

IV. CONCLUSIONS

This work presented, for the first time, direct comparison between a traditional method for analysis of neutron reflectometry measurement with analysis derived from a range of all-atom and coarse-grained molecular dynamics simulations; using the all-atom Slipid, the united-atom Berger, and the coarse-grained MARTINI potential models. It was found that the MARTINI potential model is not capable of accurately modelling the lipid monolayer system due to the limitations of the 4-to-1 beading system when applied to a carbon tail containing 18 atoms. The Berger and Slipid potential models both showed good agreement with the experimental data, however the best agreement was obtained by the traditional monolayer model. This would be expected given that the monolayer model contains many more degrees of freedom than the simulations which are severely chemically constrained by the potential model. Finally, some points from the highest resolution, Slipid, simulations were noted that may be used to improve the traditional monolayer model. These include the fact that the carbon tails were not always fully extended, and the possible desire for a non-uniform solvation of the head group region.

V. AUTHOR CONTRIBUTIONS

ACKNOWLEDGMENTS

[1] S. Llamas, E. Guzmán, A. Akanno, L. F.-P. na, F. Ortega, R. A. Campbell, R. Miller, and R. G. Rubio, J. Phys. Chem. C **122**, 4419 (2018).

[2] S. Waldie, T. K. Lind, K. Browning, M. Moulin, M. Haertlein, V. T. Forsyth, A. Luchini, G. A. Strohmeier, H. Pichler, S. Maric, and M. Cárdenas, Langmuir **34**, 472 (2018).

[3] C. Beebee, E. B. Watkins, R. M. Sapstead, V. C. Ferreira, K. S. Ryder, E. L. Smith, and A. R. Hillman, Electrochim. Acta **295**, 978 (2019).

[4] J. McCree-Grey, J. M. Cole, and P. J. Evans, ACS Appl. Mater. Interfaces **7**, 16404 (2015).

[5] G. Renaud, R. Lazzari, and F. Leroy, Surf. Sci. Rep. **64**, 255 (2009).

[6] R. A. Campbell, H. P. Wacklin, I. Sutton, R. Cubitt, and G. Fragneto, Eur. Phys. J. Plus **126**, 107 (2011).

[7] T. Arnold, C. Nicklin, J. Rawle, J. Sutter, T. Bates, B. Nutter, G. McIntyre, and M. Burt, J. Synchrotron Radiat. **19**, 408 (2012).

[8] R. D. Barker, L. E. McKinley, and S. Titmuss, in *Biophysics of Infection* (Springer US, 22016) pp. 261–282.

[9] S. Khodakarimi, M. H. Hekmatshoar, and F. Abbasi, J. Mater. Sci. Mater. Electron. **27**, 182 (2016).

[10] F. Abelès, J. Phys. Radium **11**, 307 (1950).

[11] R. A. Campbell, Y. Saaka, Y. Shao, Y. Gerelli, R. Cubitt, E. Nazaruk, D. Matyszewska, and M. J. Lawrence, J. Colloid Interface Sci. **531**, 98 (2018).

[12] T. L. Crowley, E. M. Lee, E. A. Simister, and R. K. Thomas, Physica B Condens. Matter **173**, 143 (1991).

[13] J. R. Lu, E. M. Lee, and R. K. Thomas, Acta Crystallogr. **A52**, 11 (1996).

[14] S. Bobone, Y. Gerelli, M. D. Zotti, G. Bocchinfuso, A. Farrotti, B. Orioni, F. Sebastiani, E. Latter, J. Penfold, R. Senesi, F. Formaggio, A. Palleschi, C. Toniolo, G. Fragneto, and L. Stella, BBA – Biomembranes **1828**, 1013 (2013).

[15] A. F. Miller, M. R. Wilson, M. J. Cook, and R. W. Richards, Mol. Phys. **101**, 1131 (2003).

[16] P. M. Anderson and M. R. Wilson, J. Chem. Phys. **121**, 8503 (2004).

[17] L. Darré, J. Iglesias-Fernández, A. Kohlmeyer, H. Wacklin, and C. Domene, J. Chem. Theory Comput. **11**, 4875 (2015).

[18] A. Koutsioubas, J. Phys. Chem. B **120**, 11474 (2016).

[19] A. V. Hughes, F. Ciesielski, A. C. Kalli, L. A. Clifton, T. R. Charlton, M. S. P. Sansom, and J. R. P. Webster, Acta. Crystallogr. **D72**, 1227 (2016).

[20] A. P. Dabkowska, L. E. Collins, D. J. Barlow, R. Barker, S. E. McLain, M. J. Lawrence, and C. D. Lorenz, Langmuir **30**, 8803 (2014).

[21] J. P. Jämbeck and A. P. Lyubartsev, J. Phys. Chem. B **116**, 3164 (2012).

[22] O. Berger, O. Edholm, and F. Jahnig, Biophys. J. **72**, 2002 (1997).

[23] S. J. Marrink, H. J. Risselada, S. Yefimov, D. P. Tieleman, and A. H. de Vries, J. Phys. Chem. B **111**, 7812 (2007).

[24] C. M. Hollinshead, R. D. Harvey, D. J. Barlow, J. R. P. Webster, A. V. Hughes, A. Weston, and M. J. Lawrence, Langmuir **25**, 4070 (2009).

[25] H. J. C. Berendsen, J. R. Grigera, and T. P. Straatsma, J. Phys. Chem. **91**, 6269 (1987).

[26] S. O. Yesylevskyy, L. V. Schäfer, D. Sengupta, and S. J. Marrink, PLoS Comput. Biol. **6**, 1 (2010).

[27] H. J. C. Berendsen, D. van der Spoel, and R. van Drunen, Comput. Phys. Commun. **91**, 43 (1995).

[28] E. Lindahl, B. Hess, and D. van der Spoel, J. Mol. Model. **7**, 306 (2001).

[29] D. van der Spoel, E. Lindahl, B. Hess, G. Groenhof, A. E. Mark, and H. J. C. Berendsen, J. Comput. Chem. **26**, 1701 (2005).

[30] B. Hess, C. Kutzner, D. van der Spoel, and E. Lindahl, J. Chem. Theory Comput. **4**, 435 (2008).

[31] Y. In-Chul and M. L. Berkowitz, J. Chem. Phys. **111**, 3155 (1999).

[32] L. Martínez, R. Andrade, E. G. Birgin, and J. M. Martínez, J. Comput. Chem. **30**, 2157 (2009).

[33] W. Humphrey, A. Dalke, and K. Schulten, J. Mol. Graph. **14**, 33 (1996).

[34] I. Kubo, S. Adachi, H. Maeda, and A. Seki, Thin Solid Films **393**, 80 (2001).

[35] A. R. McCluskey, A. Sanchez-Fernandez, K. J. Edler, S. C. Parker, A. J. Jackson, R. A. Campbell, and T. Arnold, Langmuir **xx**, xx (2019).

[36] A. R. McCluskey, A. Sanchez-Fernandez, K. J. Edler, S. C. Parker, A. J. Jackson, R. A. Campbell, and T. Arnold, "lipids_at_airdes," (2018).

[37] A. Nelson and S. Prescott, J. Appl. Crystallogr. **xx**, xx (2018).

[38] A. Nelson, S. Prescott, I. Gresham, and A. R. McCluskey, "refnx v0.0.17," (2018).

[39] C. Tanford, *The Hydrophobic Effect: Formation of Micelles and Biological Membranes*, 2nd ed. (John Wiley & Sons Ltd, 1980).

[40] L. Braun, M. Uhlig, R. von Klitzing, and R. A. Campbell, Adv. Colloid Interface Sci **247**, 130 (2017).